Extreme Mechanics Letters 55 (2022) 101832

Contents lists available at ScienceDirect

Extreme Mechanics Letters

journal homepage: www.elsevier.com/locate/eml

Heterogeneous digital stiffness programming

Hongcheng Tao [a], Francesco Danzi [a], Christian E. Silva [b], James M. Gibert [a,*]

[a] Advanced Dynamics and Mechanics Lab, Ray W. Herrick Laboratories, Purdue University, West Lafayette, IN, United States of America
[b] Escuela Superior Politécnica del Litoral, ESPOL, Km 30.5 Vía Perimetral, Guayaquil, Ecuador

ARTICLE INFO

Article history:
Received 4 March 2022
Received in revised form 20 May 2022
Accepted 30 June 2022
Available online 2 July 2022

Keywords:
Mechanical metamaterials
Programmable response
Vibration isolation

ABSTRACT

A heterogeneous design of mechanical metamaterial enables digital stiffness programmability. The prototype is composed of an elastomer matrix containing diamond-shaped cavities that are selectively confined along their diagonals by semi-rigid plastic beam inserts. Unit-cell perturbations caused by insert placement or removal reshape the global constitutive relation, whose lower and upper bounds correspond to configurations with all holes empty and all inserts in place, respectively, due to a gap between the elastomer and insert moduli. Bidirectional operation is accomplished by varying the orientation of the inserts, with longitudinal inserts increasing the macroscopic stiffness in compression and transverse inserts increasing that in tension. Arranged digital representations of such local insert states form the explicit encoding of global patterns, allowing both statical and in situ systematic stiffness programming with minimal mass changes. These properties establish a new paradigm for actively tuning vibration isolation systems in response to changes in the base structure's resonances.

1. Introduction

Mechanical metamaterials achieve exotic physical properties that go beyond the affine assumptions made by their chemical constituents through the use of innovative geometric design techniques [1,2]. Programmable mechanical metamaterials, in particular, represent platforms for tunable global behaviors via manipulations of unit cell deformation states either a priori in the fabrication phase or through in situ external perturbations [3–8]. Structural multistabilities such as buckling patterns of beam arrays [9–12], bistable buckling domes [13] or Kirigami slits [14–18] are widely employed for such controllable local state switching. The joint effort of unit-cell behaviors and architecture of the assembly modifies corresponding global constitutive relations toward characteristics such as quasi-zero or negative stiffness zones, negative Poisson's ratio and nonuniform curvatures for applications in energy absorption [19], vibration isolation [20], targeted shape morphing [21,22], etc. The present work introduces a heterogeneous programmable mechanical metamaterial to address several common challenges in stiffness programming strategies. First, while a comprehensive range of attainable stiffness values is generally desired for efficient programming, such bounds are inevitably limited by the fundamental mechanism of a design. For example, programmable stiffnesses of a Kirigami sheet [14] with a constant cut pattern are bounded by two extreme configurations, where all slits buckle identically. Heterogeneity is recognized as a natural approach to extend the range of material behavior [15] and a similar concept is exploited in the present work to implement a programmable stiffness range spanning between a lower bound corresponding to thin-walled collapsible structures and an upper bound of the constituent bulk material. Second, a programmable material typically operates under unidirectional loading and programming by perturbations on unit cells requires adequate deformation to be present, e.g., porous structures with arrays of thin beam elements [10] commonly work in compression and the buckling states of unit cells may be perturbed only when they are already deformed, while a Kirigami sheet functions in tension and buckling of its slits may only be controlled when a load has been applied. The present work adopts local geometric confinements [9] as the means of perturbation for both in situ and static programming capabilities, as well as bidirectional operations utilizing different confinement configurations for compression and tension. Third, geometrically admissible patterns predicted by permutations of unit cell states can be mechanically unstable in practice, which may be identified by analytical and/or experimental analysis [9,10]. This generally results from strong structural couplings among neighboring unit cells, which also causes difficulties in the independent perturbation of each unit cell so that clusters of cells sometimes need to be manipulated simultaneously. The proposed design in the present work aims to establish confidence in the physical reachability of all possible combinations of unit cell states. This allows a natural digital encoding of all programmable patterns by arranged representations of unit

* Corresponding author.
E-mail addresses: taoh@purdue.edu (H. Tao), fdanzi@purdue.edu (F. Danzi), chrsilva@espol.edu.ec (C.E. Silva), jgibert@purdue.edu (J.M. Gibert).

https://doi.org/10.1016/j.eml.2022.101832
2352-4316/

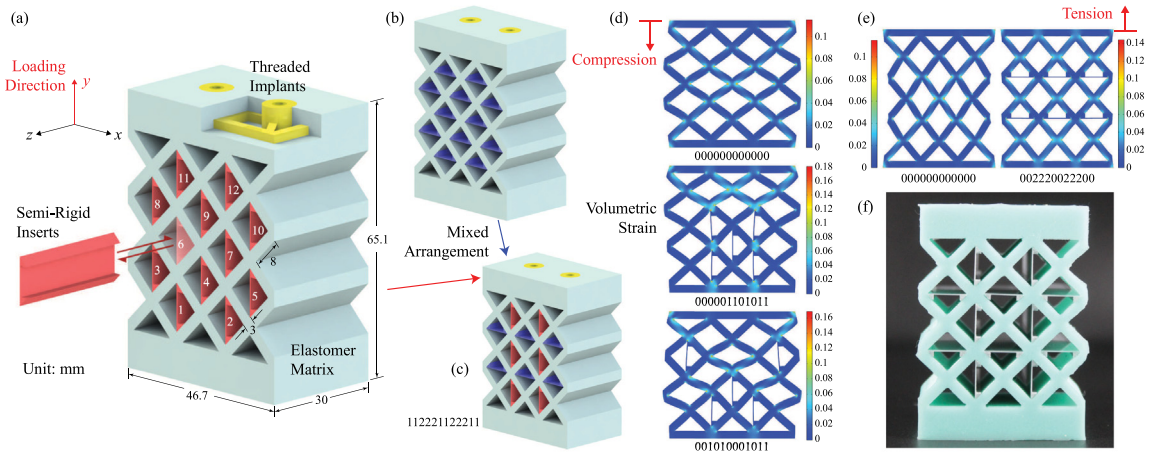

Fig. 1. Schematics of the heterogeneous programmable mechanical metamaterial. (a) Compositions and dimensions of the prototype filled with longitudinal inserts enhancing compressive stiffness, where integers indicate the corresponding digit of each unit cell for pattern encoding (the rightmost digit represents the first unit cell). (b) Prototype filled with transverse inserts enhancing tensile stiffness. (c) Prototype with mixed insert orientations. (d) Linear finite element analysis for deformations of selected patterns in compression with color map indicating magnitudes of volumetric strain. (e) Linear finite element analysis for deformations of selected patterns in tension. (f) Fabricated sample.

cell states [23], which expedites explicit modeling, analysis and optimization of programmable material behavior especially when the number of unit cells is increased. Lastly, the redundancy of such encoded global patterns due to geometric and functional symmetries limits the resolution of programming, e.g., n unit cells with identical contributions support n possible stiffnesses [24], while it will be shown that the 2-dimensional and finite (non-periodic) nature of the present design promotes a programming resolution exponentially proportional to the number of unit cells, which is usually realized in designs with structurally independent and dissimilar mechanical elements [20,25].

2. Materials and methods

The heterogeneous mechanical metamaterial accommodates stiffness programming within a wide range whose lower bound is set by a 2-dimensional collapsible elastomer matrix as a thin-walled grid formed by 12 tessellated diamond shaped holes, as demonstrated in Fig. 1a. The empty grid deforms homogeneously under uniaxial loading, as shown in Fig. 1d and Fig. 1e, where the global strain is shared uniformly among bent elastomer walls. The matrix is cast in silicone rubber (Smooth-On Mold Star 15) with embedded threaded implants for mounting onto test fixtures. Plastic beam inserts with a width of the diamond diagonal are printed in commercial PLA (modulus over 2000 MPa) which is considered semi-rigid compared to the elastomer (modulus below 0.4 MPa). Each insert can be geometrically locked in position when slid into a cavity along one of the two diagonals so that when placed longitudinally (Fig. 1a) and transversely (Fig. 1b) it confines the deformation of the four surrounding elastomer walls in global compression and tension, respectively. The effective stiffness of unit cells with inserts is transformed from that of a thin-walled elastomer grid to that of the bulk elastomer around locations of contact with the inserts, where strain is highly concentrated. The addition of inserts therefore enhances the macroscopic stiffnesses correspondingly, so that the configuration where all unit cells are filled with longitudinal inserts represents the upper bound for the global constitutive relation in compression and transverse ones that for tension. Stiffness programming between such bounds can be conducted by selective insert arrangements, whose resolution (number of achievable stiffness values) is decided by the number of independent insert patterns under geometric symmetries. A mixed pattern with inserts in both directions, as depicted in Fig. 1c, enables bidirectional stiffness programming within a comparatively narrower range. The outstanding elasticity of the silicone matrix facilitates the recovery of concentrated contact strains as well as in situ and independent placement and removal of each insert under moderate global deformations. The latter rationalizes a straightforward digital encoding scheme where each programmable insert pattern is represented by a string of integers listing the states of each unit cell with "0" for no insert, "1" for longitudinal insert and "2" for transverse, which is adopted in Fig. 1 and what follows.

Quasi-static stiffness programming in the linear region is examined with a universal test procedure where for each insert pattern the prototype undergoes three bidirectional loading cycles between terminations at 10 N reaction forces on a motorized compression test stand (Mark-10 ESM1500) at a rate of 15 mm/min, as outlined in Fig. 2a. Complementing the experimental approach, linear finite element analysis is performed in COMSOL fixing the bottom surface of the elastomer matrix and assigning a constant vertical displacement of 5 mm to the top surface in order to approximate the physical boundary conditions applied by the plastic implants, while domains of the inserts are assumed connected to the elastomer instead of applying contact boundary conditions. The prototype's deformation with different insert patterns is extracted with color maps indicating volumetric strains while the vertical reaction force integrated over the bottom surface is used to evaluate the corresponding global stiffness of each pattern.

A uniaxial model can be applied to elucidate the mechanism of the prototype's programmability under compression. Consider first an isolated digital stiffness element (unit cell), as shown in Fig. 3a, whose state can be encoded with stiffness k_{eq}^D that behaves as

$$k_{eq}^D(x) = \begin{cases} \alpha k, & \text{if } x = 0 \text{ (OFF)}, \\ (c+\alpha)k, & \text{if } x = 1 \text{ (ON)}, \end{cases} \tag{1}$$

where c is constant and α is a constant between 0 and 1, and k is a base stiffness value. Note that in tension the stiffness is $k_{eq}^D(x) = \alpha k$. The members of structure in green in Fig. 3a represent the elastomer and the member in gray represents a semi-rigid insert, so that the uniaxial behavior of the isolated unit cell can be approximated by three columns of springs connecting the four nodes, as shown in Fig. 3b. The inner column has three springs in series with the top and lower springs having a stiffness value of k

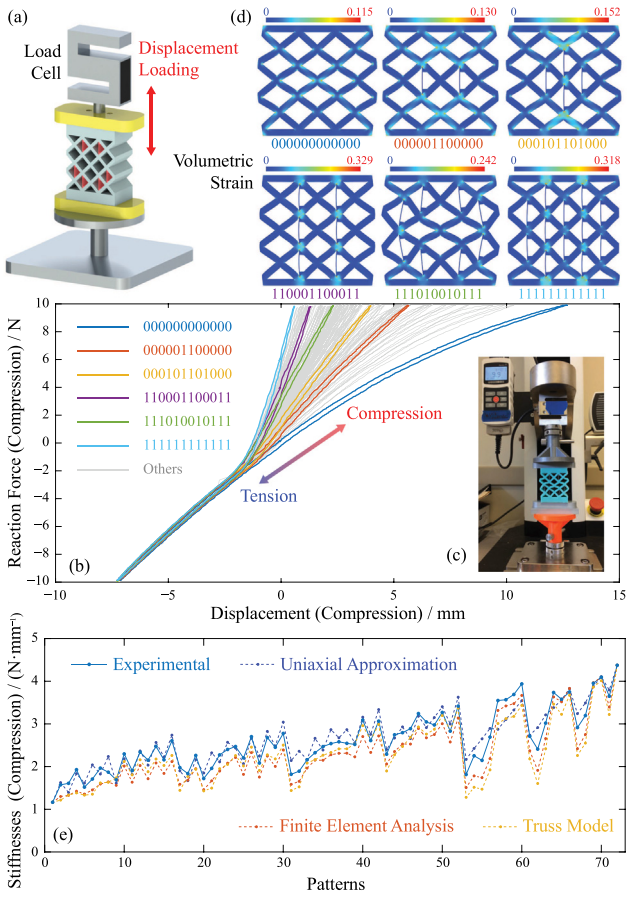

Fig. 2. Compressive stiffness programming with longitudinal inserts. (a) Quasi-static uniaxial test setup. (b) Global constitutive relations for 72 independent insert patterns. (c) Apparatus details. (d) Linear finite element analysis for deformations of highlighted patterns in compression. (e) Compressive stiffnesses of tested patterns with comparison to numerical predictions.

and middle spring has a stiffness of k_∞. The stiffnesses k and k_∞ represent the bulk elastomer, and semi-rigid insert, respectively. The outer columns represent the walls with two springs in series each having a stiffness αk. The equivalent stiffness of the system can be written as $k_{eq} = (\alpha k(2k_\infty + k) + kk_\infty)/(2k_\infty + k)$. From this expression it becomes evident that the switch-like behavior is dependent on k_∞, representing the insert. Now, if $k_\infty = 0$ then $k_{eq} \approx \alpha k$ and if $k_\infty \gg k$ then $k_{eq} \approx (1/2 + \alpha)k$. Plotting the ratio k_{eq}/k versus k_∞/k shows that the stiffness ratio value starts at a value of α and asymptotically approaches $1/2 + \alpha$, Fig. 3c, where the ratio of $k_\infty/k \gg 16$ provides a rudimentary bound to approximate the ideal digital stiffness element.

The global reaction force (and thus the global stiffness) of the prototype can then be obtained by joining the shared nodes among unit cells and assembling the stiffness matrix where states of the switchable springs are asserted according to each insert pattern, as illustrated in Fig. 4a. The uniaxial approximation can be generalized into a 2-dimensional truss model to facilitate analysis of all patterns with either longitudinal or transverse inserts, as shown in Fig. 4b, where planar nodal displacements are solved and longitudinal switchable springs are only activated when stretched while transverse ones activated only when compressed. The parameters α, k and k_∞ in both models, as well as moduli of the elastomer and insert materials in finite element analysis, are available to be fine-tuned to fit experimental datasets that are either complete or partial (as enumeration of all patterns becomes unfeasible when the number of unit cells increases).

In developing a vibration model, the archetypal relationship for the heterogeneous metamaterial under small displacement with a digital element can be represented as the force displacement curve in Fig. 5a and written as follows

$$F(\delta) = \begin{cases} k_1\delta + F_1 - k_1\delta_1, & \text{if } \delta > \delta_1 \\ k_2\delta + F_1 - k_2\delta_1, & \text{if } \delta < \delta_1 \end{cases}, \tag{2}$$

where δ is the stretch in the spring, k_1 is the linear stiffness in compression, k_2 is the linear stiffness in tension, F_1 and δ_1 are the corresponding force and displacement at the bifurcation point of the force displacement curve where the stiffness changes due to the presence of the insert. The parameters are determined by experimentally curve fitting the compression data obtained by the Mark-10 compression testing frame. The linear fits from these tests are plotted in Fig. 5b.

In order to understand the efficacy of the heterogeneous metamaterial for use in frequency programmability consider the vibration test shown in Fig. 5c and the corresponding model in Fig. 5d. The equation of motion of this system can be written as

$$\text{if } \bar{\delta}(t) > \delta_1,$$
$$m_{\text{eff}}\ddot{\bar{\delta}}(t) + c_{\text{eff}}\dot{\bar{\delta}}(t) + \mu m_{\text{eff}} g\,\text{sgn}(\dot{\bar{\delta}}(t)) + k_1\bar{\delta}(t) = k_1\delta_1 + m_{\text{eff}}g - F_1 - m_{\text{eff}}\ddot{x}_{\text{B}}(t), \tag{3a}$$
$$\text{if } \bar{\delta}(t) < \delta_1,$$
$$m_{\text{eff}}\ddot{\bar{\delta}}(t) + c_{\text{eff}}\dot{\bar{\delta}}(t) + \mu m_{\text{eff}} g\,\text{sgn}(\dot{\bar{\delta}}(t)) + k_2\bar{\delta}(t) = k_2\delta_1 + m_{\text{eff}}g - F_1 - m_{\text{eff}}\ddot{x}_{\text{B}}(t), \tag{3b}$$

where $\bar{\delta}(t) = x(t) - x_{\text{B}}(t)$, is defined as the compression in the material, $x(t)$ is the absolute motion of the proof mass, $\ddot{x}_{\text{B}}(t)$ is the base acceleration defined as $\ddot{x}_{\text{B}}(t) = G\sin\omega t$, G is the amplitude of acceleration, ω is the frequency of excitation, m_{eff} is the sum of the mass of the insert, equivalent mass of the elastomer, and the proof mass, c_{eff} is damping coefficient of the material, g is the gravitational constant. The coefficient between the components of the rail guide is denoted as μ. The effective mass and stiffness in tension are adjusted from their nominal values. This was done to: (1) match the experimental resonant frequency, and (2) account for the inserts slightly losing contact when the elastomer vibrates when the structure is in tension. It is hypothesized that the individual inserts act as locally resonant structures whose interactions reduce the apparent mass of the material [26,27]. The changes in these parameters along with coefficient of friction, and damping coefficient are determined from fitting two experimental frequency response function (FRF) curves. The Eqs. (3a) and (3b) are solved numerically in Matlab using the solver ODE45. The FRF curves were obtained by varying the forcing frequency and solving the equations of motion for each frequency until the system reached steady state. At steady state the peak amplitudes of response were recorded.

3. Results and discussion

Considering longitudinal inserts only and assuming transverse mirror symmetry, 72 independent patterns are tested where for each the global displacement-reaction relation is extracted from the third cycle, as plotted in Fig. 2b with deformations of the highlighted patterns illustrated in Fig. 2d. These patterns exhibit nearly identical mechanical behaviors in tension while spreading densely in the compression domain, the calculated stiffnesses of which match closely the predictions by finite element analysis, the uniaxial simplification and the 2-dimensional truss model discussed previously, as enumerated in Fig. 2e with patterns sorted

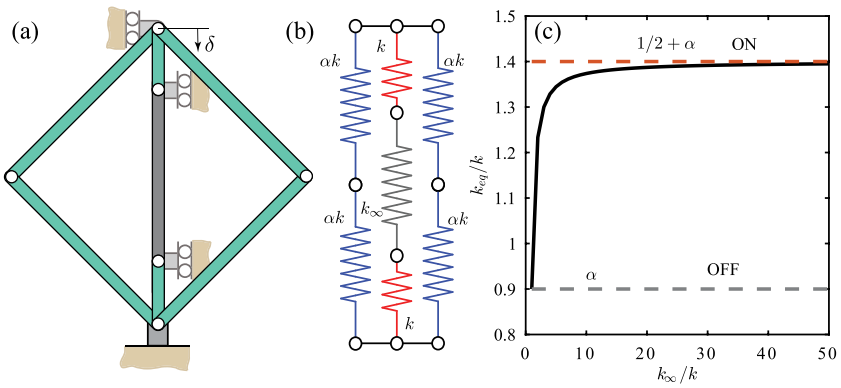

Fig. 3. Behavior of unit cell. (a) Interpretation of the unit cell as a truss approximation. (b) Simplification of the truss model as a uniaxial approximation. (c) Plot of equivalent stiffness ratio to insert stiffness ratio with bounds set as digital stiffness values.

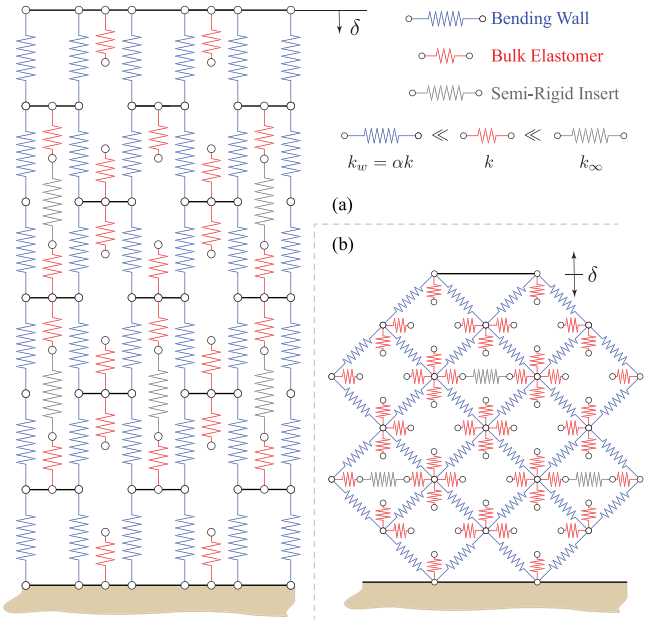

Fig. 4. Spring network approximation of the heterogeneous metamaterial. (a) Uniaxial model for prototype with all longitudinal inserts under compression. (b) Generalization to a 2-dimensional truss model.

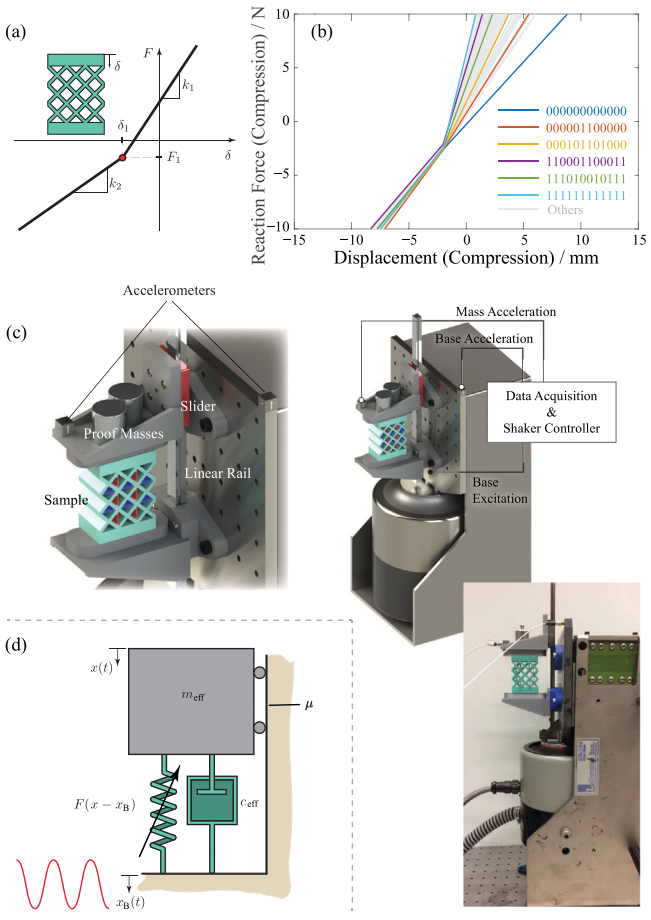

Fig. 5. Dynamic lumped parameter model of the metamaterial. (a) Bilinear curve fit of all experimental data, selected curves are highlighted. (b) Pictorial description of bilinear force(F)-displacement(δ) plot. (c) Vibration test setup on an electrodynamic shaker. (d) Bilinear lumped parameter model.

according to their ternary codes translated into decimal numbers. A remarkable gap is observed between the lowest linear stiffness of 1.16 N/mm where all inserts are removed and the highest limit of 4.37 N/mm where all holes are filled with longitudinal inserts.

The 72 patterns experimentally investigated are those that are transversely symmetric while not vertically mirroring each other, e.g., pattern 110000000000 is considered identical to 000000000011 so that only one of them (000000000011) is examined. The number of such independent transversely symmetric patterns can be calculated by letting $(2a-1)$ be the number of rows (of unit cells) in a sample and $(b-1)$ be the number of unit cells in the bottom row ($a, b \in \mathbb{Z}^+$) so that the total number of unit cells is $n = 2ab - a - b$. The number of all transversely symmetric patterns is $p_1 = 2^{ab-\frac{1}{2}b^*}$, among which the number of those that are also vertically symmetric is $p_2 = 2^{\frac{1}{4}\left[a^*(b-1)^*+(a-1)^*b^*\right]}$, where $x^* = x$ if x is even while $x^* = x+1$ if x is odd ($x \in \mathbb{Z}^+$), so that the number of independent transversely symmetric patterns is $p = \frac{1}{2}(p_1 - p_2) + p_2 = \frac{1}{2}(p_1 + p_2)$. For example, the tested prototype has $a = b = 3$ so that $n = 12$, $p_1 = 2^7 = 128$, $p_2 = 2^4 = 16$ and therefore $p = 72$. In general, assuming $a = b \geq 2$ there is $p = 2^{\frac{1}{2}\left(a^2-2\right)}\left[2^{\frac{1}{2}a(a-1)} + 1\right]$ if a is even, while $p = 2^{\frac{1}{2}\left(a^2-3\right)}\left[2^{\frac{1}{2}a(a-1)} + 1\right]$ if a is odd, indicating that the stiffness programming resolution is exponentially proportional to the number of unit cells which is now $n = 2a(a-1)$. This relation between the number of unit cells n and the number of independent patterns p is further depicted in Fig. 6 while Fig. 7 enumerates finite-element predictions of all achievable stiffness

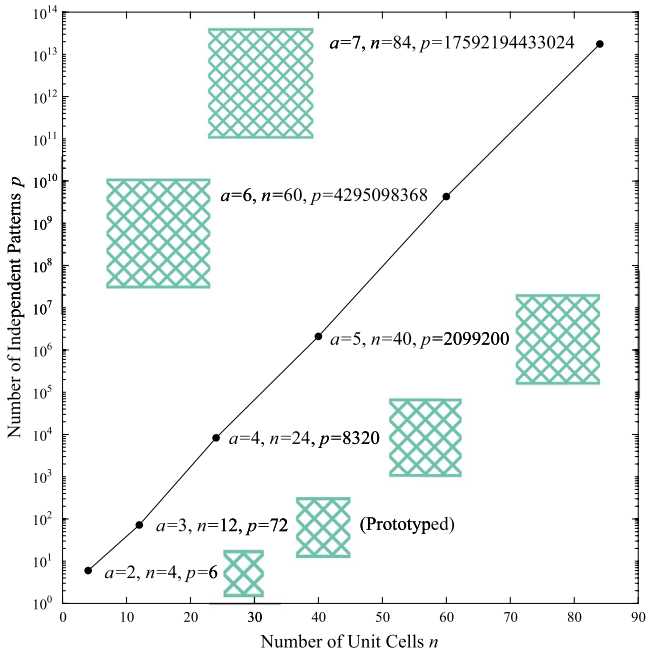

Fig. 6. Number of independent transversely symmetric patterns with identical insert orientation, as a function of total number of unit cells in a sample.

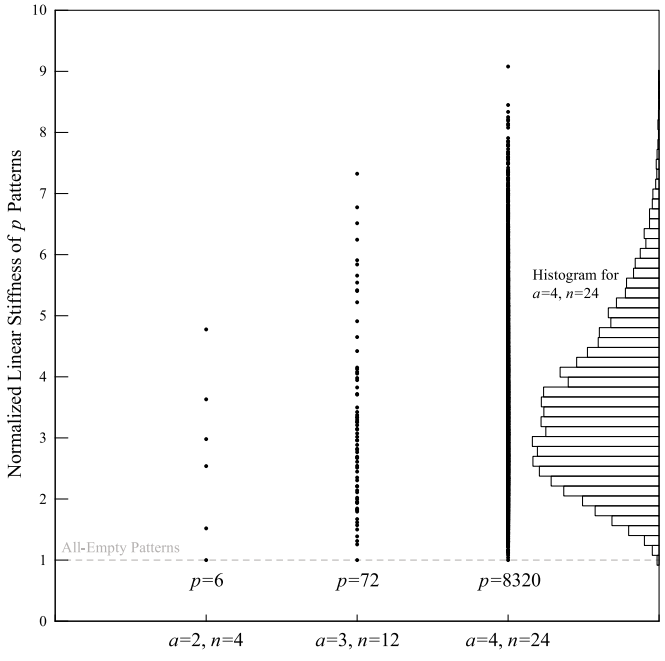

Fig. 7. Linear stiffness values by finite element analysis for all independent (transversely symmetric) patterns with longitudinal inserts, normalized by that of the all-empty pattern, for samples with 4, 12 and 24 unit cells.

values normalized by that of the all-empty patterns for $a = 2$, 3 and 4, including a histogram for the 8320 values for $a = 4$.

Meanwhile, selected patterns with only transverse inserts are tested as shown in Fig. 8a, featuring overlapped macroscopic behaviors in compression but programmability in the tension region instead. Furthermore, bidirectional stiffness programming with selected patterns involving mixed insert orientations displays bilinear constitutive relations as a superposition of the independent contributions by longitudinal and transverse inserts in the

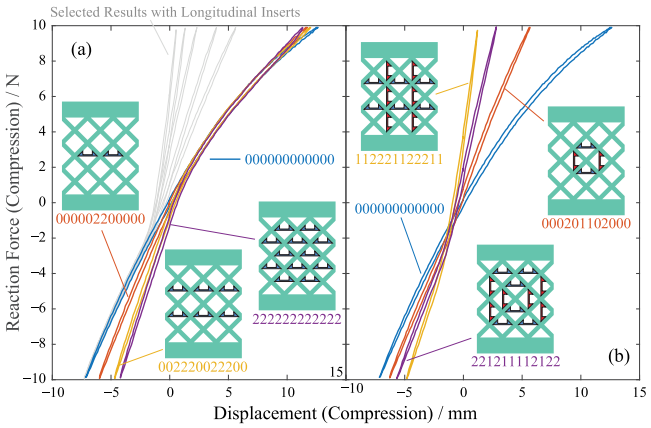

Fig. 8. Tensile and bidirectional stiffness programming. Experimental global constitutive relations for (a) selected transverse insert patterns, and (b) selected mixed insert patterns.

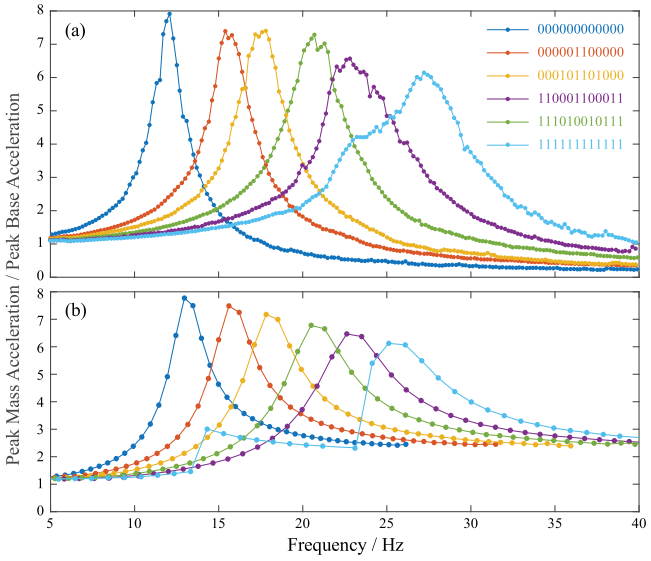

Fig. 9. Transfer functions generated with sinusoidal dwell excitation series. (a) Experimental transfer functions from base to proof mass acceleration. (b) Theoretical transfer functions from base to proof mass acceleration.

compression and tension regions, respectively, as illustrated in Fig. 8b.

Vast availability of programmable stiffnesses allows the material platform to be used in applications such as adaptive vibration isolation systems. When supporting an adequate mass upon a massive base, the prototype is anticipated to be capable of adjusting the system's resonant frequency up to doubling, given roughly the ratio between the upper and lower stiffness bounds observed in Fig. 2e and that the mass of inserts has a minimal effect. This is investigated on an electrodynamic shaker for selected patterns highlighted in Fig. 2b with only longitudinal inserts, as portrayed in Fig. 5c. The steady-state acceleration of a proof mass (0.2 kg), vertically connected via the programmed prototype onto the shaker base undergoing a series of sinusoidal excitations with constant magnitude $0.1g$ (g is gravitational acceleration) dwelling at discrete frequencies, is recorded as in Fig. 9a. The static preload by gravity of the proof mass along with the low excitation magnitude ensures operation in the close-to-linear compression region. Results imply programmable resonant frequencies covering a broad band roughly from 12 Hz to 27 Hz,

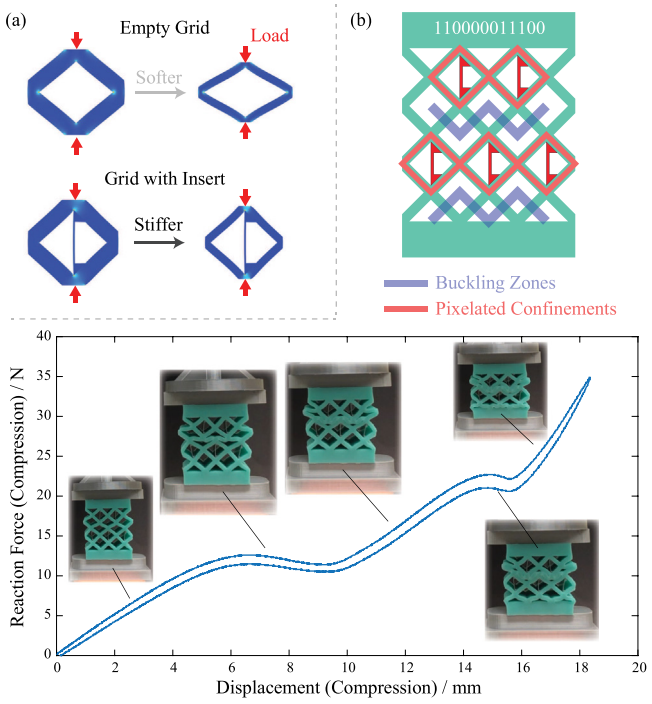

Fig. 10. Interpretations of the fundamental mechanism. (a) Improved programmable range by reducing elastomer thickness. (b) Nonlinear piecewise stiffness programming with consecutive buckling zones.

revealing potentials in rapid tuning of vibration isolation units in situations where resonance of base structures may shift in time.

Fig. 9b is a theoretical plot of the frequency response function between the base acceleration to the proof mass acceleration. For all configurations tests the theoretical responses agree qualitatively to the experimental ones in Fig. 9a. The magnitudes of vibration and the resonant peaks have similar values. Note that in both the experimental case and in the model given in Eqs. (3a) and (3b) the FRF for configuration 111111111111 has a distorted resonant peak. The model captured the presence of the distortion but does not match the shape of the FRF curve. In this configuration, the model indicated that the distortion occurred over a limited frequency range and was due to the metamaterial switching from vibrating strictly below δ_1, to vibrating in a region above and below δ_1.

The above clarifies the proposed implementation of a stiffness programming strategy that achieves universal stability of geometrically defined input patterns and thus a direct encoding scheme, both static and in situ independent perturbation of unit cells in bidirectional operations, as well as a vast range of programmable stiffnesses. It is worth noting that such a ratio between upper and lower stiffness bounds can be extended without replacement of constituent materials but by narrowing the elastomer matrix walls, as conceptually shown in Fig. 10a, which reduces the structural stiffness of a collapsible unit cell with no insert but hardens one with an insert by cutting the volume of bulk elastomer around contact points. Meanwhile, the prototype can be further adapted as a platform for programming more sophisticated mechanical and dynamic behaviors by allowing freedom in the design of inserts for varieties of functions beyond rigid confinements. An example of this adaptation is to note that a variety of stiffness states can be realized by manipulating the geometry of the insert to a shape beyond a beam. Moreover, nonlinear deformation regions may also be explored following a separate interpretation of the design, in which zones of buckling beam arrays are indirectly programmed via opposite rigid confinement constructions using inserts. Successive collapses and self contact of elastomer zones divided by confinements dominate the structure's behavior in different deformation phases, as shown in Fig. 10b, which sees potentials in microscopic modifications of nonlinear constitutive relations of an extensive grid by programming clusters of unit cells as groups of pixelated confinement geometries.

4. Conclusion

Digital stiffness programming is realized using a 2-dimensional heterogeneous mechanical metamaterial featuring semi-rigid removable inserts to emulate both series and parallel arrangements of dissimilar springs, where each unit cell contributes uniquely to reach a resolution of linear stiffness programmability exponentially proportional to the number of unit cells. The design addresses common challenges in stiffness programming mechanisms and exhibits flexibilities as a platform for tuning complex macroscopic mechanical and dynamic behaviors by adopting various unit cell functions given the freedom of deploying any geometrically lockable functional insert. Additionally, the platform through confined bucking exhibits the ability to program nonlinear constitutive relationships.

Declaration of competing interest

The authors declare that they have no known competing financial interests or personal relationships that could have appeared to influence the work reported in this paper.

Acknowledgments

The authors would like to acknowledge the Purdue Research Foundation (PRF), and the National Science Foundation, United States under Grant: CMMI 1662925 and CAREER Award: CMMI 2145803 for the financial support provided.

Appendix A. Supplementary data

Supplementary material related to this article can be found online at https://doi.org/10.1016/j.eml.2022.101832.

References

[1] K. Bertoldi, V. Vitelli, J. Christensen, M. Van Hecke, Flexible mechanical metamaterials, Nat. Rev. Mater. 2 (11) (2017) 1–11.
[2] J.U. Surjadi, L. Gao, H. Du, X. Li, X. Xiong, N.X. Fang, Y. Lu, Mechanical metamaterials and their engineering applications, Adv. Energy Mater. 21 (3) (2019) 1800864.
[3] H. Fang, S.-C.A. Chu, Y. Xia, K.-W. Wang, Programmable self-locking origami mechanical metamaterials, Adv. Mater. 30 (15) (2018) 1706311.
[4] C. Coulais, E. Teomy, K. De Reus, Y. Shokef, M. Van Hecke, Combinatorial design of textured mechanical metamaterials, Nature 535 (7613) (2016) 529–532.
[5] P. Wang, F. Casadei, S. Shan, J.C. Weaver, K. Bertoldi, Harnessing buckling to design tunable locally resonant acoustic metamaterials, Phys. Rev. Lett. 113 (1) (2014) 014301.
[6] J.L. Silverberg, A.A. Evans, L. McLeod, R.C. Hayward, T. Hull, C.D. Santangelo, I. Cohen, Using origami design principles to fold reprogrammable mechanical metamaterials, Science 345 (6197) (2014) 647–650.
[7] Y. Wang, B. Ramirez, K. Carpenter, C. Naify, D.C. Hofmann, C. Daraio, Architected lattices with adaptive energy absorption, Extreme Mech. Lett. 33 (2019) 100557.
[8] B. Haghpanah, L. Salari-Sharif, P. Pourrajab, J. Hopkins, L. Valdevit, Multistable shape-reconfigurable architected materials, Adv. Mater. 28 (36) (2016) 7915–7920.
[9] B. Florijn, C. Coulais, M. van Hecke, Programmable mechanical metamaterials, Phys. Rev. Lett. 113 (17) (2014) 175503.

[10] E. Medina, P.E. Farrell, K. Bertoldi, C.H. Rycroft, Navigating the landscape of nonlinear mechanical metamaterials for advanced programmability, Phys. Rev. B 101 (6) (2020) 064101.
[11] A. Rafsanjani, A. Akbarzadeh, D. Pasini, Snapping mechanical metamaterials under tension, Adv. Mater. 27 (39) (2015) 5931–5935.
[12] C. El-Helou, R.L. Harne, Exploiting functionally graded elastomeric materials to program collapse and mechanical properties, Adv. Energy Mater. 21 (12) (2019) 1900807.
[13] J.P. Udani, A.F. Arrieta, Programmable mechanical metastructures from locally bistable domes, Extreme Mech. Lett. 42 (2021) 101081.
[14] Y. Yang, M.A. Dias, D.P. Holmes, Multistable kirigami for tunable architected materials, Phys. Rev. Mater. 2 (11) (2018) 110601.
[15] N. An, A.G. Domel, J. Zhou, A. Rafsanjani, K. Bertoldi, Programmable hierarchical kirigami, Adv. Funct. Mater. 30 (6) (2020) 1906711.
[16] A. Rafsanjani, D. Pasini, Bistable auxetic mechanical metamaterials inspired by ancient geometric motifs, Extreme Mech. Lett. 9 (2016) 291–296.
[17] Y. Tang, G. Lin, S. Yang, Y.K. Yi, R.D. Kamien, J. Yin, Programmable Kiri-Kirigami metamaterials, Adv. Mater. 29 (10) (2017) 1604262.
[18] D.-G. Hwang, M.D. Bartlett, Tunable mechanical metamaterials through hybrid kirigami structures, Sci. Rep. 8 (1) (2018) 1–8.
[19] S. Shan, S.H. Kang, J.R. Raney, P. Wang, L. Fang, F. Candido, J.A. Lewis, K. Bertoldi, Multistable architected materials for trapping elastic strain energy, Adv. Mater. 27 (29) (2015) 4296–4301.
[20] Q. Zhang, D. Guo, G. Hu, Tailored mechanical metamaterials with programmable quasi-zero-stiffness features for full-band vibration isolation, Adv. Funct. Mater. (2021) 2101428.
[21] R. Guseinov, C. McMahan, J. Pérez, C. Daraio, B. Bickel, Programming temporal morphing of self-actuated shells, Nature Commun. 11 (1) (2020) 1–7.
[22] L. Jin, A.E. Forte, B. Deng, A. Rafsanjani, K. Bertoldi, Kirigami-inspired inflatables with programmable shapes, Adv. Mater. 32 (33) (2020) 2001863.
[23] B. Haghpanah, H. Ebrahimi, D. Mousanezhad, J. Hopkins, A. Vaziri, Programmable elastic metamaterials, Adv. Energy Mater. 18 (4) (2016) 643–649.
[24] T. Chen, M. Pauly, P.M. Reis, A reprogrammable mechanical metamaterial with stable memory, Nature 589 (7842) (2021) 386–390.
[25] W. Li, F. Wang, O. Sigmund, X.S. Zhang, Digital synthesis of free-form multimaterial structures for realization of arbitrary programmed mechanical responses, Proc. Natl. Acad. Sci. 119 (10) (2022) e2120563119.
[26] S. Yao, X. Zhou, G. Hu, Experimental study on negative effective mass in a 1D mass–spring system, New J. Phys. 10 (4) (2008) 043020.
[27] G.W. Milton, J.R. Willis, On modifications of Newton's second law and linear continuum elastodynamics, Proc. R. Soc. A 463 (2079) (2007) 855–880.